PERGAMON

International Journal of Engineering Science 38 (2000) 215–238

International Journal of Engineering Science

www.elsevier.com/locate/ijengsci

Mathematical model of pulsatile blood flow in a distensible aortic bifurcation subject to body acceleration

S. Chakravarty *, P.K. Mandal, A. Mandal

Department of Mathematics, Visva-Bharati University, Santiniketan 731 235, India

Received 18 August 1997; accepted 9 December 1998

Abstract

The present analytical investigation has been dealt with pulsatile flow characteristics of blood in a distensible bifurcated artery having a stenosis when it is subjected to whole body acceleration. The geometry of the bifurcated artery developed by the present first two authors (S. Chakravarty, P.K. Mandal, Int. J. Eng. Sci. 35 (1997) 409–422) has been used to carry out the present analysis. It incorporates the arterial wall motion by treating it as an anisotropic, linear viscoelastic incompressible material. The unsteady flow mechanism in the bifurcated artery subject to a pulsatile pressure gradient arising from the normal functioning of the heart as also the body acceleration is presented mathematically. The effect of the surrounding connective tissues on the motion of the arterial wall is also paid due consideration. The effect of the wall distensibility on the bifurcated flow phenomena has been accounted for through suitably formulated continuity conditions. The equations governing the motion of the system are sought in the Laplace transform space and their relevant solutions are obtained in the transformed domain by using an appropriate finite difference scheme. Their inversions to the physical domain lead to calculate the velocity profile of the flowing blood in both the parent and the daughter arteries together with the arterial wall displacements. From the computational results based on the short-time-range approximations, one may disclose that the body acceleration and the wall distensibility do not change the flow patterns in the parent aorta, but there is a drastic change in the daughter artery, which in turn, causes an appreciable increase in the shear stresses developed on both the parent and its daughter arterial walls. The pulsatile flow helps inducing the wall shear stress to change the direction over a cycle which may be important in the mechanism of atherosclerosis.

* Corresponding author. Tel.: +91 03463 52751; fax: +91 03463 52672.
E-mail address: genusr@rbharat.ernet.in (S. Chakravarty)

0020-7225/00/$ – see front matter
PII: S0020-7225(99)00022-1

1. Introduction

The study of blood flow in the aortic bifurcation is of great clinical interest both with respect to genesis and the diagnostics of atherosclerosis – an arterial constriction causing physiological flow disorder leading to the malfunction of the cardiovascular system. Such arterial constrictions usually appear around curvatures, junctions and bifurcations of large and medium arteries, where the flow patterns are essentially complicated. The complex flow disorder poses great concern to distinguish these disturbances from normal flow behaviour in these regions. It is a well documented fact that the arterial walls in these critical regions are exposed to both high and low shear stresses due to the adhesion and depositions of blood platelets and lipids. Liepsch and Moravec [2] and Liepsch [3] propounded from their experimental studies that in regions with high shear stresses, the blood cells are damaged or their surface is changed and then the particles stick to the wall followed by a deposition in regions with low shear stresses. In order to have a complete understanding of the flow through aortic bifurcation from the physical point of view, one needs to be fully conversant with the haemodynamic behaviour of blood together with the rheological properties of the vascular wall material under physiological state of strain. Moreover, under normal physiological conditions, the blood transportation in the circulatory system depends entirely on the pumping action of the heart producing a pressure gradient throughout the arterial system. However, there may be some exceptional situations under which humans experience whole body accelerations. Such situations generally arise while riding in a vehicle or while flying in a spacecraft. External accelerations of considerable amplitudes imparted to the human body can influence the bifurcated flow characteristics and that can cause serious problems in the cardiovascular system leading to the impairment of certain physiological functions.

Quite a good number of theoretical and experimental studies relevant to this domain of biomechanics have been carried out to investigate the significant role of haemodynamics in atherogenesis. A comprehensive review concerning the present field of research has been successfully conducted by Lou and Yang [4]. However, there have been only a few experimental studies performed to determine the effect of wall distensibility on the wall shear stress and other local flow conditions [2,5,6]. Many investigators recognized the importance of the viscoelastic property of the arterial wall. Any disregard to the viscoelasticity of the vessel wall can result in an underestimation of both phase velocity and damping as pointed out by Reuderink et al. [7]. In fact the viscoelastic arterial wall model yields results closer to normal physiological fact than the elastic wall model and a dissipative wall is more effective than a dissipative fluid in eliminating the high frequency oscillations. Lou and Yang [8] have investigated the effect of arterial wall distensibility on the flow field at the aortic bifurcation numerically, from a computer simulation.

An attempt is made in the present theoretical investigation to evaluate some of the important characteristics of pulsatile blood flow in a distensible aortic bifurcation subject to body acceleration using an appropriate mathematical model. This study considers the bifurcated arterial wall to be of linear anisotropic viscoelastic material as pointed out by Patel and Vaishnav [9] from their dynamic experiment and blood flowing through it to be Newtonian. It is commonly believed that the effect of non-Newtonian property of blood is small in larger arteries, where the shear rate is high. Particular emphasis has been put on the effect of the surrounding connective tissues on the motion of the arterial wall in order to have the dynamic response of the bifurcated arterial system under in vivo situation. The body acceleration expressible in terms of unit functions is such that it

builds up from zero to a maximum value at a uniform rate, remains constant there for some time and thereafter drops down to zero at a uniform rate. A suitable time-dependent geometry developed by Chakravarty and Mandal [1] has been chosen for the present investigation. The parent aorta is assumed to have a mild stenosis in its lumen (cf. Clark et al. [10]) while the daughter ones are free from any constriction. The bifurcation is considered to be symmetrical about the trunk axis and the appropriate curvatures at the lateral junctions and the flow divider are introduced so as to improve resemblance to the in vivo situation in a sense that when a vessel bifurcates, it does it gradually. The cylindrical coordinate system has been taken for analytical formulation. The governing equations of motion of the arterial wall together with the flow phenomena are sought first in the Laplace transform space and their solutions are obtained in the transformed domain subject to appropriate boundary conditions by using a finite difference scheme. Their inversions to the physical domain lead to calculate the flow velocity, the flow rate and the wall shear stresses in both the parent and the daughter arteries. With the introduction of the short-time-range approximations an extensive quantitative analysis is performed through numerical computations of the desired quantities presented graphically at the end of the paper followed by a complete discussion so as to justify the validity of the present mathematical model.

2. Formulation of the problem

For the analytical formulation of the present mathematical model, the following assumptions are imposed.

- The arteries forming bifurcations are symmetrical about the trunk axis and straight circular cylinders of finite length
- The parent aorta possesses a single mild stenosis in its lumen.
- The arterial wall material is linear anisotropic viscoelastic and incompressible.
- A linear viscoelastic spring-dashpot model is introduced to simulate the tissues surrounding the arterial wall.
- Blood is a homogeneous Newtonian fluid of constant density.
- Curvatures are introduced at the lateral junctions and the flow divider so that one can rule out the possibility of the presence of any discontinuity causing non-existent flow separation zones.
- The external body acceleration is included which seems to have a significant effect on the flow characteristics of blood in accelerating or decelerating blood flow in that arterial bifurcation.

Let (r,θ,z) be the coordinates of a material point in the cylindrical polar coordinate system where the z-axis is taken along the axis of trunk while (r,θ) are taken along the radial and the circumferential directions respectively. The geometry of the bifurcated artery (cf. Fig. 1) in the presence of stenosis is constructed mathematically of which the outer wall geometry is described by

$$(R_1(z,t)=\begin{cases} a_1(t), & 0\leqslant z\leqslant d', \quad d'+l_0\leqslant z\leqslant z_1,\\ \left[a-\frac{4\tau_m}{l_0^2}\{l_0(z-d')-(z-d')^2\}\right]a_1(t), & d'\leqslant z\leqslant d'+l_0,\\ \left[a+r_0-\sqrt{r_0^2-(z-z_1)^2}\right]a_1(t), & z_1\leqslant z\leqslant z_2,\\ [2r_1\sec\beta+(z-z_2)\tan\beta]a_1(t), & z_2\leqslant z\leqslant z_{\max}, \end{cases} \tag{1}$$

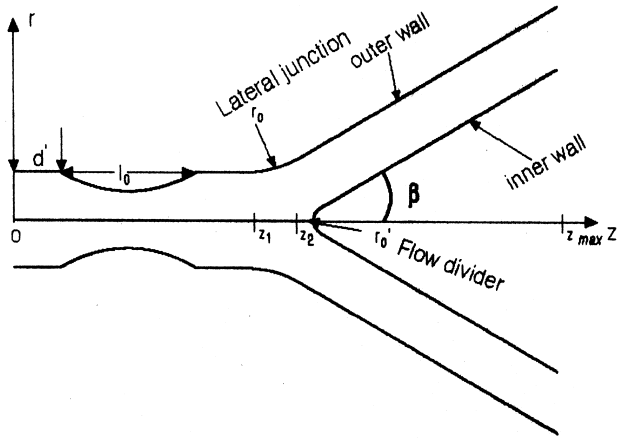

Fig. 1. Schematic diagram of the stenosed bifurcated artery.

while that for the inner half is given by

$$R_2(z,t) = \begin{cases} 0, & 0 \leqslant z \leqslant z_3, \\ \sqrt{r_0'^2 - (z - z_3 - r_0')^2}\, b_1(t), & z_3 \leqslant z \leqslant z_3 + r_0'(1 - \sin\beta), \\ [r_0' \cos\beta + z_4] b_1(t), & z_3 + r_0'(1 - \sin\beta) \leqslant z \leqslant z_{\max}, \end{cases} \tag{2}$$

where $R_1(z,t)$ and $R_2(z,t)$ are the respective radii of the outer and the inner wall, a the radius of the parent artery, r_1 the radius of the daughter artery, (r_0, r_0') the radii of curvatures for the lateral junction and the flow divider respectively, l_0 the length of the stenosis at a distance d' from the origin, z_1 the location of the onset of the lateral junction, z_2 the offset of the lateral junction, z_3 the apex, β, half the bifurcation angle and τ_m represents the maximum height of the stenosis at $z = d' + l_0/2$. Here, $z_{\max}$ designates the finite length of the bifurcated artery under consideration.

Moreover, the parameters involved in the above expressions (1) and (2) may be defined as

$$\begin{aligned} a_1(t) &= 1 - (\cos\omega t - 1) k \exp(-k\omega t), \\ b_1(t) &= \frac{1}{a_1(t)}, \\ z_2 &= z_1 + (a - 2r_1 \sec\beta) \frac{\sin\beta}{\cos\beta - 1}, \\ z_4 &= \{z - z_3 - r_0'(1 - \sin\beta)\} \tan\beta, \\ r_0 &= \frac{a - 2r_1 \sec\beta}{\cos\beta - 1}, \quad r_0' = \frac{(z_3 - z_2)\sin\beta}{1 - \sin\beta} \end{aligned} \tag{3}$$

and $z_3 = z_2 + q$, where q is chosen to be a small number lying in the range $0.1 \leqslant q \leqslant 0.5$ for compatibility of the geometry and k is a constant.

Suppose at time $t > 0$, the flow in the aortic bifurcation is subjected to a single cycle of body acceleration $F(t)$ (cf. Fig. 2) expressible in terms of unit functions which may be represented mathematically as

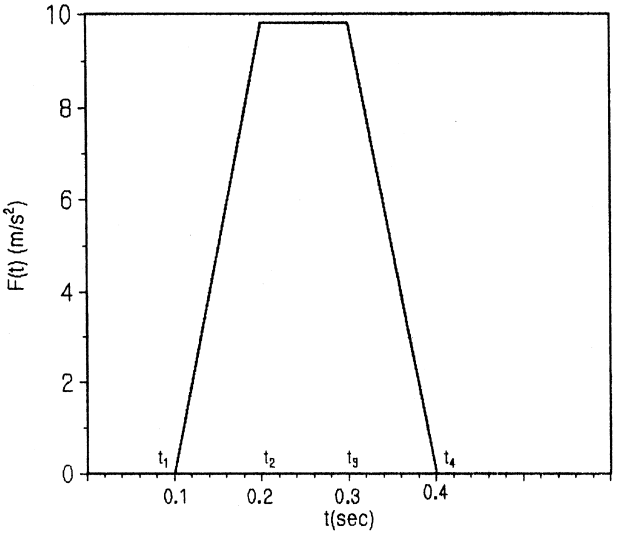

Fig. 2. Schematic representation of the body acceleration.

$$F(t) = a_0(t-t_1)u(t-t_1) - a_0(t-t_2)u(t-t_2) - a_1(t-t_3)u(t-t_3) + a_1(t-t_4)u(t-t_4), \tag{4}$$

where a_0 and a_1 are the respective acceleration and deceleration rates as shown in Fig. 2, t_1 is the time of application of the body acceleration, $(t_2 - t_1)$ is the build-up time, $(t_4 - t_3)$ is the climb-down time and t_4 is the moment when the acceleration ceases to apply; $u(t)$ represents a step function and t, the generic time.

The governing equations of motion of the bifurcated arterial wall when it is subjected to inertial forces and the forces of constraint representing the reactions of the surrounding connective tissues may be put in the form

$$(\sigma_z - \sigma_\theta)\frac{\partial R}{\partial z} + R\frac{\partial \sigma_z}{\partial z} - \left(M_0\frac{\partial^2 \xi}{\partial t^2} + C_l\frac{\partial \xi}{\partial t} + K_l\xi\right) - \frac{\partial R}{\partial z}\left(M_0\frac{\partial^2 \eta}{\partial t^2} + C_r\frac{\partial \eta}{\partial t} + K_r\eta\right) = 0, \tag{5}$$

$$\frac{\sigma_\theta}{r}\left[1 + \left(\frac{\partial R}{\partial z}\right)^2\right]^{-1/2} - \frac{\partial^2 R}{\partial z^2}\left[1 + \left(\frac{\partial R}{\partial z}\right)^2\right]^{-3/2}\sigma_z - \frac{1}{R}\left[1 + \left(\frac{\partial R}{\partial z}\right)^2\right]^{-1/2} \times \left[\frac{\partial R}{\partial z}\left(M_0\frac{\partial^2 \xi}{\partial t^2} + C_l\frac{\partial \xi}{\partial t} + K_l\xi\right) - \left(M_0\frac{\partial^2 \eta}{\partial t^2} + C_r\frac{\partial \eta}{\partial t} + K_r\eta\right)\right] = 0 \tag{6}$$

in which $M_0 = \rho_0 h + M_a$ where ρ_0 and h are the mass density and thickness of the vessel wall respectively. (ξ, η) represent the generic displacement components of the vessel wall along the axial and the radial direction, respectively, in a sense that the axial displacement components for the outer and the inner walls should be read as ξ_1 and ξ_2 corresponding to the replacement of R in the above Eqs. (5) and (6) by R_1 and R_2, respectively. $(\sigma_z, \sigma_\theta)$ are the respective viscoelastic stress components acting along the longitudinal and circumferential directions. K_l, C_l and M_a represent

(per unit area) the spring coefficient, the frictional coefficient of the dashpot and the additional mass of he mechanical model, respectively, [11,12] of the longitudinal tethering and K_r, C_r are those in the radial direction.

Let us consider the flow in the arterial bifurcation to be unsteady, axisymmetric, laminar, one dimensional and fully developed, the basic equation of motion governing such flow subject to body acceleration in the absence of any radial /rotational flow may be as

$$\rho\frac{\partial w}{\partial t} = \mu\left(\frac{\partial^2 w}{\partial r^2} + \frac{1}{r}\frac{\partial w}{\partial r}\right) - \frac{\partial p}{\partial z} + \rho F(t), \tag{7}$$

where $w = w(r, z, t)$ is the axial velocity of the flowing blood, p the pressure, ρ the density and μ the viscosity of blood.

Since our attention is focused on the axial flow behaviour of blood, we have further

$$\frac{\partial p}{\partial r} = 0 = \frac{\partial p}{\partial \theta}. \tag{8}$$

These relations yield $p = p(z, t)$. The form of the pressure gradient present in Eq. (7) appearing due to pumping action of the heart, has been taken from Burton [13] as

$$-\frac{\partial p}{\partial z} = A_0 + A_1\cos\omega t, \tag{9}$$

where A_0 is the constant amplitude of the pressure gradient, A_1 is the amplitude of the pulsatile component giving rise to systolic and diastolic pressure; $\omega = 2\pi f_p$, f_p is the pulse frequency.

3. Constitutive relations

As per experimental observations, the arterial wall may be treated as an anisotropic, linear viscoelastic incompressible membrane shell and the constitutive relations for the axisymmetric deformation may have the following form

$$\sigma_z(t) = -p_1(t) + \int_0^t K_1^z(t-\tau)\dot{E}_z(\tau)\,\mathrm{d}\tau, \tag{10}$$

$$\sigma_\theta(t) = -p_1(t) + \int_0^t K_1^\theta(t-\tau)\dot{E}_\theta(\tau)\,\mathrm{d}\tau, \tag{11}$$

where E_z, E_θ are the strain components along the longitudinal and the circumferential directions, respectively, p_1 being the hydrostatic pressure and (K_1^z, K_1^θ) define the material relaxation functions.

4. Boundary conditions

The velocity gradient of the streaming blood along the axis of the bifurcated artery till its apex may be assumed to be equal to zero, that is, there is no shear rate of the fluid along the trunk axis, which may be written as

$$\frac{\partial w}{\partial r} = 0 \quad \text{on } r = 0,\ 0 \leqslant z \leqslant z_3. \tag{12}$$

Considering that the blood particles adhere to the arterial wall surface, the velocity boundary condition on the outer wall is given by

$$w(r,z,t) = \frac{\partial \xi_1}{\partial t} \quad \text{on } r = R_1(z,t), \tag{13}$$

while that on the inner half (daughter) is taken to be

$$w(r,z,t) = \frac{\partial \xi_2}{\partial t} \quad \text{on } r = R_2(z,t),\ \ z_3 \leqslant z \leqslant z_{\max}. \tag{14}$$

Also, it is assumed that there is a non-zero velocity of the flowing blood when the system is at rest. That means,

$$w(r,z,t) = w_0 \quad \text{at } t = 0. \tag{15}$$

5. Method of solution

Introducing the constitutive relations (10) and (11) into (5) and (6) and employing the short-time-range approximation, one finds

$$\frac{\partial R}{\partial z}\left[K_1^z(0)E_z(t) - K_1^\theta(0)E_\theta(t)\right] + RK_1^z(0)\frac{\partial E_z}{\partial z}$$

$$-\left(M_0\frac{\partial^2 \xi}{\partial t^2} + C_l\frac{\partial \xi}{\partial t} + K_l\xi\right) - \left(M_0\frac{\partial^2 \eta}{\partial t^2} + C_r\frac{\partial \eta}{\partial t} + K_r\eta\right)\frac{\partial R}{\partial z} = 0 \tag{16}$$

and

$$\frac{1}{R}\left[-p_1 + K_1^\theta(0)E_\theta(t)\right]\left[1 + \left(\frac{\partial R}{\partial z}\right)^2\right]^{-1/2} - \frac{\partial^2 R}{\partial z^2}\left[1 + \left(\frac{\partial R}{\partial z}\right)^2\right]^{-3/2}\left[-p_1 + K_1^z(0)E_z(t)\right]$$

$$-\frac{1}{R}\left[1 + \left(\frac{\partial R}{\partial z}\right)^2\right]^{-1/2}\left[\frac{\partial R}{\partial z}\left(M_0\frac{\partial^2 \xi}{\partial t^2} + C_l\frac{\partial \xi}{\partial t} + K_l\xi\right) - \left(M_0\frac{\partial^2 \eta}{\partial t^2} + C_r\frac{\partial \eta}{\partial t} + K_r\eta\right)\right] = 0. \tag{17}$$

Eqs. (16) and (17) are now sought to Laplace transform space which should be read as

$$\frac{d\bar{R}}{dz}\left[K_1^z(0)\frac{d\bar{\xi}}{dz}-K_1^\theta(0)\frac{\bar{\eta}}{\bar{R}}\right]+\bar{R}K_1^z(0)\frac{d^2\bar{\xi}}{dz^2}-(M_0s^2+C_ls+K_l)\bar{\xi}$$

$$-\frac{d\bar{R}}{dz}(M_0s^2+C_rs+K_r)\bar{\eta}=0 \tag{18}$$

and

$$\frac{1}{\bar{R}}\left[-\bar{p}_1+K_1^\theta(0)\frac{\bar{\eta}}{\bar{R}}\right]\left[\left[1+\left(\frac{\partial\bar{R}}{\partial z}\right)^2\right]^{-1/2}-\frac{d^2\bar{R}}{d\xi^2}\left[1+\left(\frac{\partial\bar{R}}{\partial z}\right)^2\right]^{-3/2}\left[-p_1+K_1^z(0)\frac{d\bar{\xi}}{dz}\right]\right.$$

$$\left.-\frac{1}{\bar{R}}\left[1+\left(\frac{\partial\bar{R}}{\partial}\right)^2\right]^{-1/2}\left[\frac{d\bar{R}}{dz}(M_0s^2+C_ls+K_l)\bar{\xi}-(M_0s^2+C_rs+K_r)\bar{\eta}\right]\right]=0, \tag{19}$$

where the variables with an overbar designate their Laplace transforms and s, the transformation variable.

Eq. (19) yields

$$\bar{\eta}=\frac{1}{f_1}\left(f_2+f_3\bar{\xi}+f_4\frac{d\bar{\xi}}{dz}\right), \tag{20}$$

in which the expressions for the coefficients f_i's $(i=1,2,3,4)$ are included in Appendix A.

Inserting Eq. (20) into Eq. (18) one can express the following second order differential equation in $\bar{\xi}$ as

$$g_{11}\frac{d^2\bar{\xi}}{dz^2}+g_{12}\frac{d\bar{\xi}}{dz}+g_{13}\bar{\xi}+g_{14}=0, \tag{21}$$

where g_{ik}'s $(k=1,2,3,4)$ have their expressions included in Appendix A.

Before we search for the solutions of Eqs. (20) and (21) let us now focus our attention on the haemodynamic factors only. Generally in a problem concerning the coupling of the fluid mechanics with the arterial wall mechanics, $R_1(z,t)$ and $R_2(z,t)$ would not be given but instead, could be computed as a part of the solution of the coupled problem. Here both $R_1(z,t)$ and $R_2(z,t)$ are prescribed and hence the introduction of a radial coordinate transformation, given by

$$x=\frac{r-R_2}{R_1-R_2}=\frac{r-R_2}{R}, \tag{22}$$

possess the effect of immobilizing the bifurcated arterial wall in the transformed coordinate x. Here, $R(z,t)=R_1(z,t)-R_2(z,t)$.

Using this transformation, Eq. (7) takes the following form

$$\rho\frac{\partial w}{\partial t}=\mu\left[\frac{1}{R^2}\frac{\partial^2 w}{\partial x^2}+\frac{1}{R(xR+R_2)}\frac{\partial w}{\partial x}\right]-\frac{\partial p}{\partial z}+\rho F(t)+\frac{\rho}{R}\left(x\frac{\partial R}{\partial t}+\frac{\partial R_2}{\partial t}\right)\frac{\partial w}{\partial x}, \tag{23}$$

where $w=w(x,z,t)$. The boundary conditions (12)–(15) are also transformed in concert with Eq. (22) to

$$\frac{\partial w}{\partial x}=0 \text{ on } x=0 \text{ for } z<z_3, \tag{24}$$

$$w(x,z,t)=\frac{\partial \xi_1}{\partial t} \text{ on } x=1 \tag{25}$$

$$w(x,z,t)=\frac{\partial \xi_2}{\partial t} \text{ on } x=0 \text{ for } z\geqslant z_3, \tag{26}$$

$$w(x,z,0)=w_0 \text{ at } t=0. \tag{27}$$

Eq. (23) governing flow together with the boundary conditions (24)–(26) are all sought in the Laplace transform (LT) space which should be read as

$$\frac{\mu}{\bar{R}^2}\frac{\partial^2 \bar{w}}{\partial x^2}+\left[\frac{\mu}{\bar{R}(x\bar{R}+\bar{R}_2)}+\frac{\rho}{\bar{R}}\{(x\bar{R}+\bar{R}_2)s-x\bar{R}(z,0)-R_2(z,0)\}\right]\frac{\partial \bar{w}}{\partial x}$$

$$-\rho s\bar{w}=\frac{\mathrm{d}\bar{p}}{\mathrm{d}z}-\rho w_0-\rho\bar{F}(s), \tag{28}$$

$$\frac{\partial \bar{w}}{\partial x}=0 \text{ on } x=0 \quad \text{for } z<z_3, \tag{29}$$

$$\bar{w}(x,z,s)=s\bar{\xi}_1 \quad \text{on } x=1, \tag{30}$$

$$\bar{w}(x,z,s)=s\bar{\xi}_2 \quad \text{on } x=0 \quad \text{for } z\geqslant z_3, \tag{31}$$

in which

$$\frac{\mathrm{d}\bar{p}}{\mathrm{d}z}=-\left(\frac{A_0}{s}+\frac{A_1 s}{s^2+w^2}\right) \tag{32}$$

$$\text{and } \bar{F}(s)=\frac{1}{s^2}[a_0(\mathrm{e}^{-st_1}-\mathrm{e}^{-st_2})-a_1(\mathrm{e}^{-st_3}-\mathrm{e}^{-st_4})]. \tag{33}$$

6. Finite difference approximation

In order to solve the wall Eqs. (20) and (21) and Eq. (28) of flow subject to the prescribed conditions, the finite difference approximations have been taken based on the central difference formula so that the Eqs. (21) and (28) can be expressed as the following difference equations, given by

$$\left[\frac{(g_{11})_i}{(\Delta z)^2}-\frac{(g_{12})_i}{(2\Delta z)}\right]\bar{\xi}_{i-1}+\left[-2\frac{(g_{11})_i}{(\Delta z)^2}+(g_{13})_i\right]\bar{\xi}_i+\left[\frac{(g_{11})_i}{(\Delta z)^2}+\frac{(g_{12})_i}{(2\Delta z)}\right]\bar{\xi}_{i+1}=-(g_{14})_i \tag{34}$$

$$a_{i,j}\bar{w}_{i,j-1}+b_{i,j}\bar{w}_{i,j}+c_{i,j}\bar{w}_{i,j+1}=d_{i,j}, \tag{35}$$

where the respective expressions for $a_{i,j}, b_{i,j}$ and $c_{i,j}$ are included in Appendix A while that for $d_{i,j}$ is given on the right-hand side of Eq. (28). Also the notation $(\ )_i$ appearing in Eq. (34), denotes that expressions (34) and (35) are uncoupled and of tridiagonal type which can be solved by the Thomas algorithm where one defines $x_j=(j-1)\Delta x, j=1(1)N+1$ and $z_i=(i-1)\Delta z, i=1(1)M+1$ for the entire bifurcated artery under consideration in which Δx and Δz are the increments in the radial and the axial directions, respectively. Also, the boundary conditions (29)–(31) have their finite difference representations in the LT space, given by

$$\bar{w}_{i,1}=\bar{w}_{i,2} \quad \text{for } z_i<z_3, \tag{36}$$

$$\bar{w}_{i,N+1}=s\bar{\xi}_{1i} \quad \text{for all } i \tag{37}$$

$$\bar{w}_{i,1}=s\bar{\xi}_{2i} \quad \text{for } z_i\geqslant z_3. \tag{38}$$

After having obtained the solutions of Eqs. (34) and (35) in the transformed space, the volumetric flow rate $(\bar{Q}_p,\bar{Q}_d)$ for both the parent $(z<z_3)$ aorta and the daughter $(z\geqslant z_3)$ arteries can be determined, respectively, in the LT space as

$$\bar{Q}_p=2\pi\bar{R}_i\left[\bar{R}_i\int_0^1 x_j\bar{w}_{i,j}\,\mathrm{d}x_j+\bar{R}_{2j}\int_0^1\bar{w}_{i,j}\,\mathrm{d}x_j\right], \tag{39}$$

$$\bar{Q}_d=\pi\bar{R}_i\left[\bar{R}_i\int_0^1 x_j\bar{w}_{i,j}\,\mathrm{d}x_j+\bar{R}_{2i}\int_0^1\bar{w}_{i,j}\,\mathrm{d}x_j\right]. \tag{40}$$

The transformed wall shear stresses $\left[(\bar{\tau}_p)_i,(\bar{\tau}_{\mathrm{od}})_i\right]$ on the parent and the external daughter wall can be derived and computed right from Eq. (7) whose expressions are not shown here for the sake of brevity, while that on the inner wall of the daughter vessel may be obtained in the transformed space as

$$(\bar{\tau}_{\mathrm{id}})_i=-\frac{\mu}{\bar{R}_i\Delta_x}\left(\bar{w}_{i,2}-s\bar{\xi}_{2i}\right) \text{ for } z\geqslant z_3. \tag{41}$$

Here the suffixes "od"' and "id" indicate the outer daughter and the inner daughter, respectively.

Knowing all the solutions in the transformed space, the inversion is carried out numerically by means of Gaussian quadrature formulae in order to have their measure quantitatively in the physical domain and hence to perform a complete discussion of the results obtained in the following section. The corresponding steady state analysis has also been carried out and computed numerically but their respective expressions are not presented for the sake of brevity.

7. Numerical results and discussion

With a view to examining the validity of the present mathematical model, we have undertaken a specific numerical illustration using the existing data for the various physical parameters encountered in the analysis. The numerical computations have been performed with the objectives to estimate the flow velocity, the flow rates, the wall shear stresses and the vessel wall displacements for both the parent aorta and the daughter arteries together with the effect of body acceleration on them quantitatively. The effects of arterial wall distensibility on those physical quantities and their steady state response are however not ruled out from the present bifurcated flow phenomena. For this purpose, the following data have been taken (Milnor [14], Lou and Yang [4], Mirsky [15], Young et al. [16]):

$a = 7.5$ mm, $l_0 = 15$ mm, $d' = 5$ mm, $z_{\max} = 60$ mm, $\tau_m = 0.4\ a$, $f_p = 1.2$ Hz, $\rho = 1.05 \times 10^3$ kg m^{-3}, $\mu = 0.035$ P, $\beta = 30^0$, $z_4 = 25$ mm, $r_1 = 0.51\ a$, $A_0 = 100$ kg m^{-2} s^{-2}, $A_1 = 0.2\ A_0$, $\kappa = 0.1$, $\rho_0 = 1.05 \times 10^3$ kg m^{-3}, $h = 0.02$ mm, $K_1^z(t) = 6.4 \times 10^4$ N m^{-2}, $K_1^\theta(t) = [494 + 46\exp(-0.23t^{0.57})] \times 10^2$ N m^{-2}, $M_1 = 0.70$, C $= 550$, $K = 1.6 \times 10^6$, $M_0 = M_1 a\rho_0$, $C_l = \mu$C/a, $K_l = \mu^2 K/a^3\rho_0$, $a_0 = 0.981$ m s$^{-3} = a_1$, $t_1 = 0.1$ s, $t_2 = 0.2$ s, $t_3 = 0.3$ s, $t_4 = 0.4$s.

Also, it is intuitively assumed that $C_r \simeq C_l$ and $K_r \simeq K_l$ due to non-availability of the information regarding these parameters.

The finite difference scheme has been found to converge with the spacings $\Delta z = 0.025$ and $\Delta x = 0.01$. The necessary convergence of the results obtained has been achieved with the desired degree of accuracy for a grid size of 240×100 and the results are finally portrayed through the Figs. 3–16 followed by a complete discussion in order to substantiate the applicability of the present model.

Fig. 3 illustrates the behaviour of the velocity profile of the streaming blood in the parent aorta at a specific location of $z = 12.5$ mm where it assumes its constriction maximum for three different time periods. The present figure also includes the corresponding results for three different cases: (i) by disregarding the presence of external body acceleration; (ii) by ignoring the vessel wall distensibility and (iii) by bringing the system into the steady state which are noted with distinguishable marks. All the curves are found to be diminishing from there maxima at the axis as one moves away from it and finally they approach a minimum value on the wall surface where the flow velocity completely merges with the velocity of the moving arterial wall. The time-variant nature of flow velocity reflects closely the input pulsatile pressure gradient, as anticipated. The presence of body acceleration causes the flow velocity of blood to enhance significantly and thus its effect on the flow velocity can be quantified through the numerical comparison between the relevant curves of the figure. The enhancement of the maximum flow velocity at the axis is nearly fivefold while that is reduced considerably towards the vicinity of the vessel wall surface. The flow velocity appears to enhance appreciably in the absence of any arterial wall motion so that the effect of wall

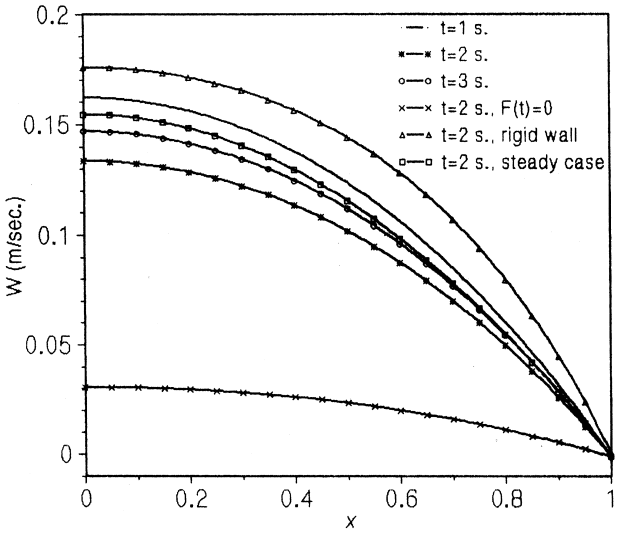

Fig. 3. Axial velocity profile for the parent artery at $z = 12.5$ mm for different time periods ($\tau_m = 0.4$a, $\beta = 30°$).

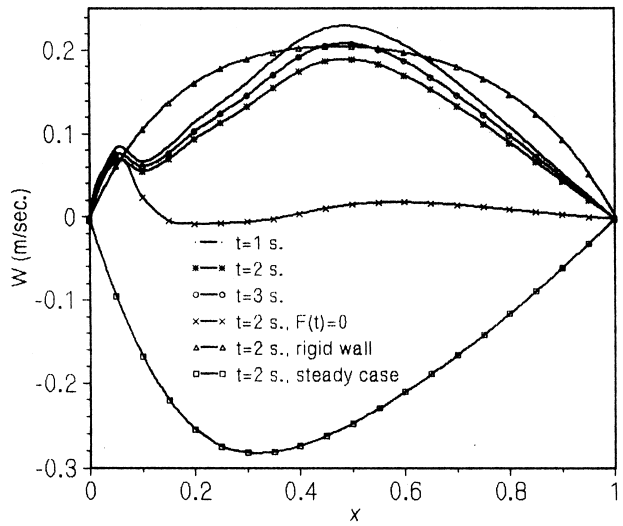

Fig. 4. Axial velocity profile for the daughter artery at $z = 40$ mm for different time periods ($\tau_m = 0.4$ a, $\beta = 30°$).

distensibility on the flow velocity can be estimated quantitatively through a comparative study of the first and the fifth curves from the top of the present figure. The corresponding steady state results plotted in this figure with an increasing trend over those in the unsteady state further help indicating a substantial effect on the velocity profile of the streaming blood. Thus one may conclude after thorough study over all the results of the present figure that the body acceleration, the arterial wall distensibility and the unsteady state of the system should be regarded as key role players in such a bifurcated flow model.

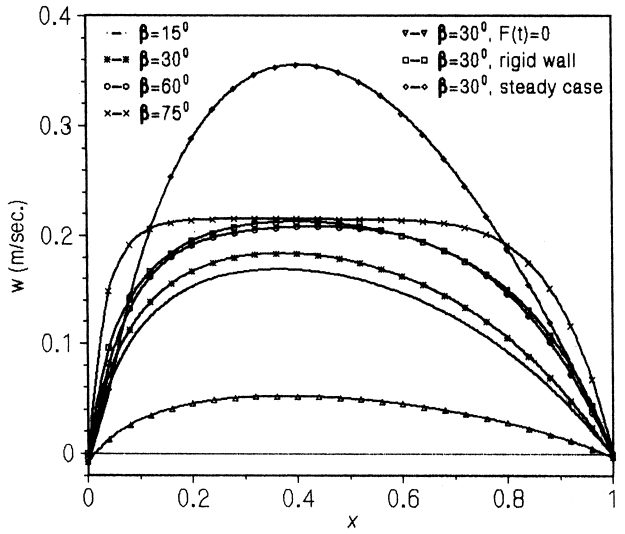

Fig. 5. Axial velocity profile for the apex for different value of β at $t = 2$ s.

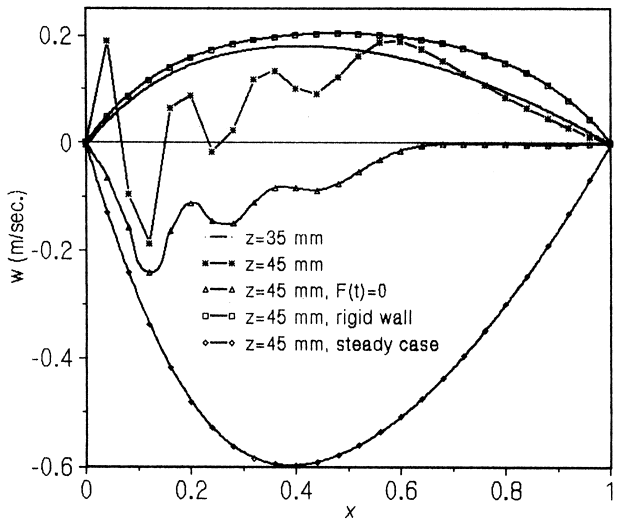

Fig. 6. Axial velocity profile for the daughter artery at different axial positions ($\beta = 30°$, $t = 2$ s.

Unlike the nature of the velocity profile in the parent aorta, the flow profile in the daughter arteries is changed drastically as observed from the results of Fig. 4 consisting of six distinct curves plotted at a particular location of $z = 40$ mm. Three similar curves with a little fluctuations corresponding to different time periods show their localised maxima near the inner wall followed by their overall maxima near the median wall surface and finally approach a minimum value on the outer wall surface in the presence of body acceleration and vessel wall distensibility. If one withdraws the body acceleration from the system, the velocity profile experiences some distortions

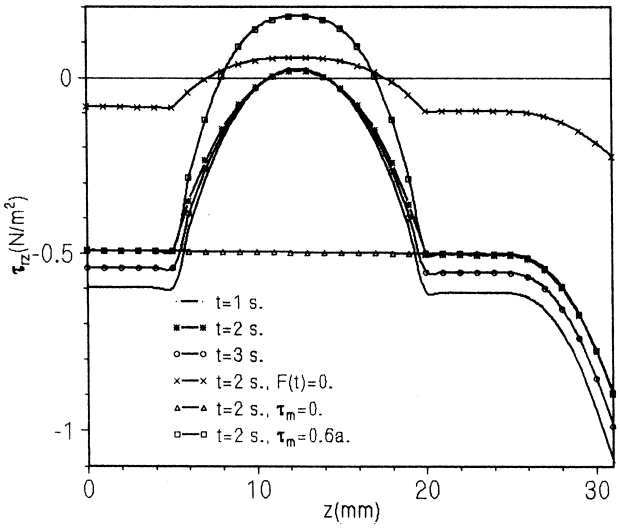

Fig. 7. Wall shear stress distribution for the parent aorta at different time periods ($\beta = 30°$, $\tau_m = 0.4a$).

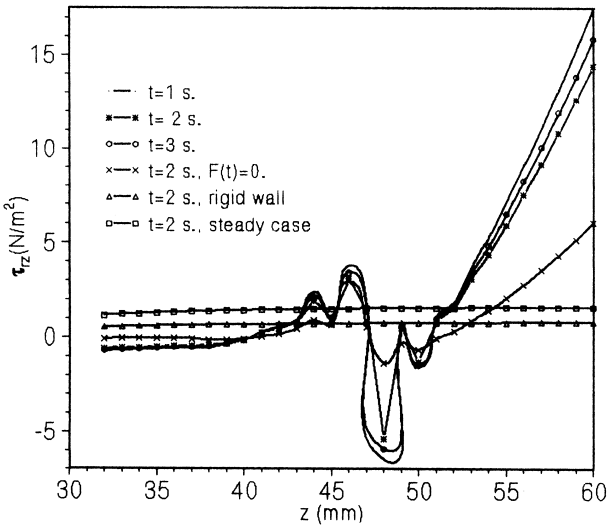

Fig. 8. Wall shear stress distribution for the daughter outer wall at different time periods ($\beta = 30°$).

in the daughter arteries and attains its peak near the inner wall followed by a back flow region in the vicinity of the inner wall and then approaches minimum value on the outer wall surface by traversing the path of positive non-zero values distal to the separation zone. In the absence of the arterial wall motion, the flow pattern becomes entirely different where neither any flow reversal occurs nor any peak forms near the inner wall surface and, instead, the velocity increases symmetrically from zero on the inner wall surface, attains a peak near the median wall and then gradually drops to zero on the outer wall. In contrast to this, the flow velocity becomes all time

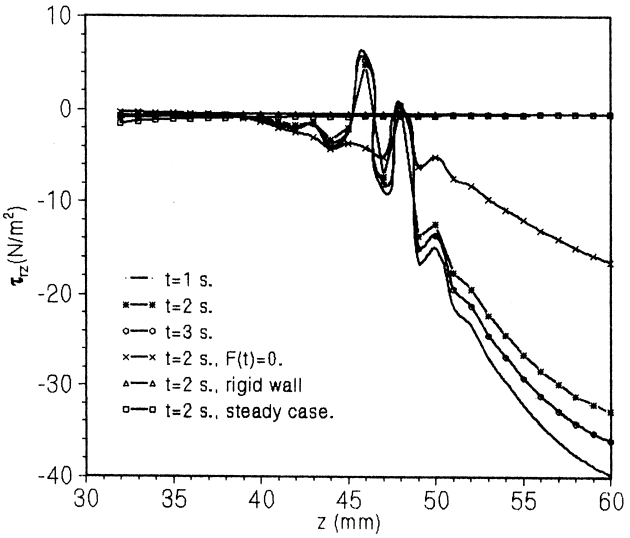

Fig. 9. Wall shear stress distribution for the daughter inner wall at different time periods ($\beta = 30°$).

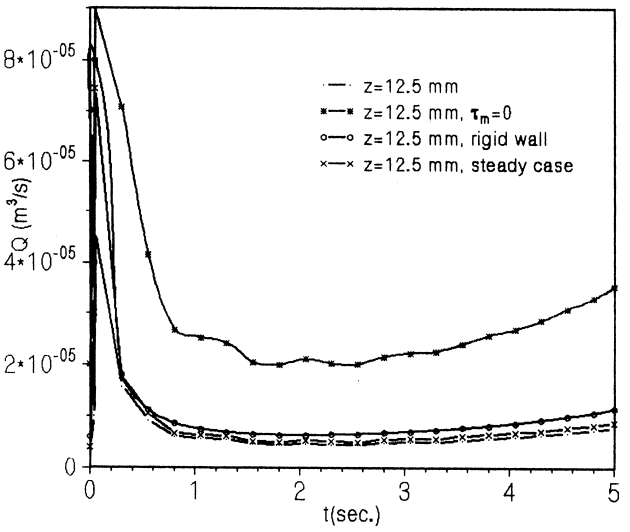

Fig. 10. Variation of the flow rate with time for the parent aorta at $\beta = 30°$.

negative with a minimum value near the inner wall when the system is brought to the steady state. Examining the results of Figs. 3 and 4, it may be of some importance to note that the body acceleration, the vessel wall distensibility and the pulsatile flow influence the velocity pattern in daughter arteries more than that in the parent aorta.

Fig. 5 includes the results for the flow velocity pattern at the apex for various bifurcation angles in the physiologic range at a particular instant of $t = 2$ s. The present figure also incorporates the results by disregarding the external body acceleration, by ignoring the vessel wall distensibility

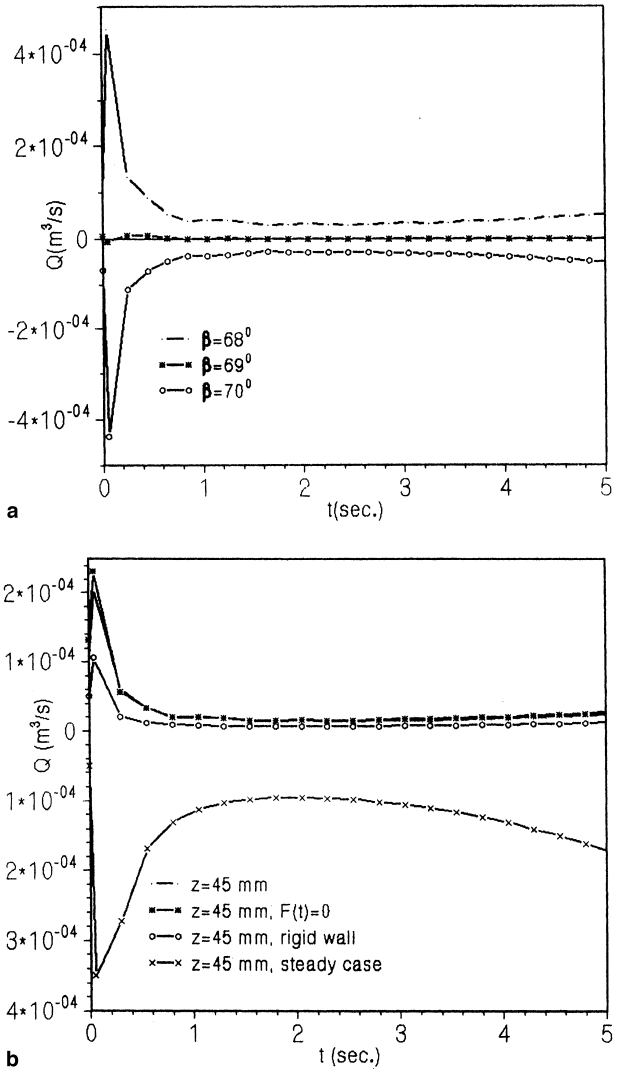

Fig. 11. (a) Variation of the rate of flow with time for the daughter artery for different β at $z = 45$ mm. (b) Varation of the rate of flow with time for the daughter artery at $\beta = 30°$.

and by plugging the system into a steady state so as to have proper understanding of their influences on the flow pattern at the apex. It is observed that with the increase of the bifurcation angle, the usual velocity pattern of parabolic nature is perturbed considerably and gradually gets flattened. The bifurcation angle influences the Coriolis force significantly and the secondary flow becomes prominent in the present study because of a large bifurcation angle and a relatively flat flow profile. This observation is in good agreement qualitatively with that of Fukushima et al. [17]. In the absence of the external body acceleration at the aortic bifurcation the profile gets its magnitudes significantly lowered while it appears to have gained higher magnitude when the vessel wall distensibility is totally disregarded. The corresponding result for a steady state exhibit an all

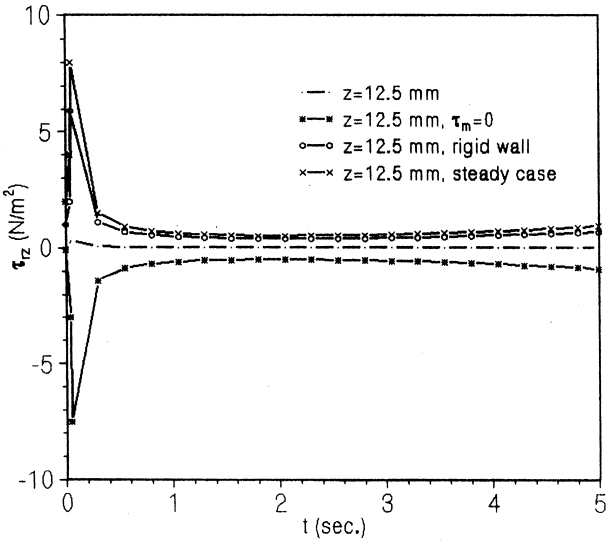

Fig. 12. Variation of the wall shear stress with time for the parent aorta at $\beta = 30°$.

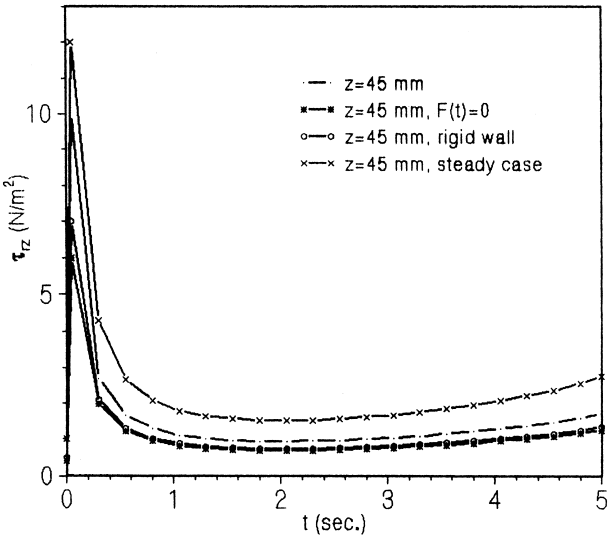

Fig. 13. Variation of the wall shear stress with time for the daughter outer wall at $\beta = 30°$.

time increase over those for unsteady state considered in the present study. One may note that the velocity profile for the steady case deviates from a parabolic profile less than the unsteady flow. The steady flow has sharper velocity peak than the one in unsteady flow. Such observation agrees qualitatively well with that of Lou and Yang [18] who studied the same theoretically by computer simulation.

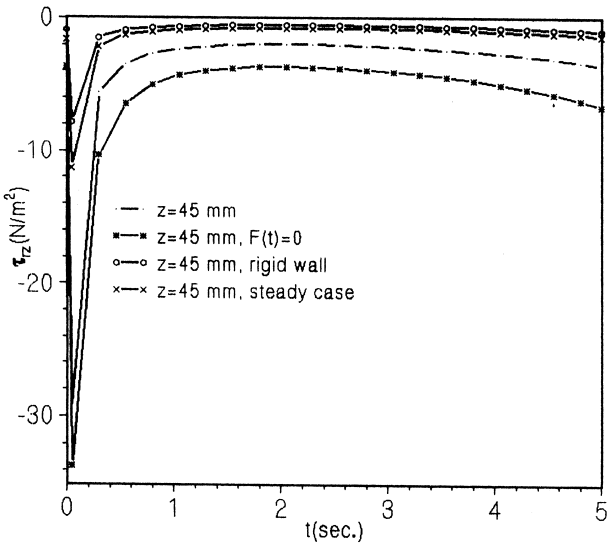

Fig. 14. Variation of the wall shear stress with time for the daughter inner wall at $\beta = 30°$.

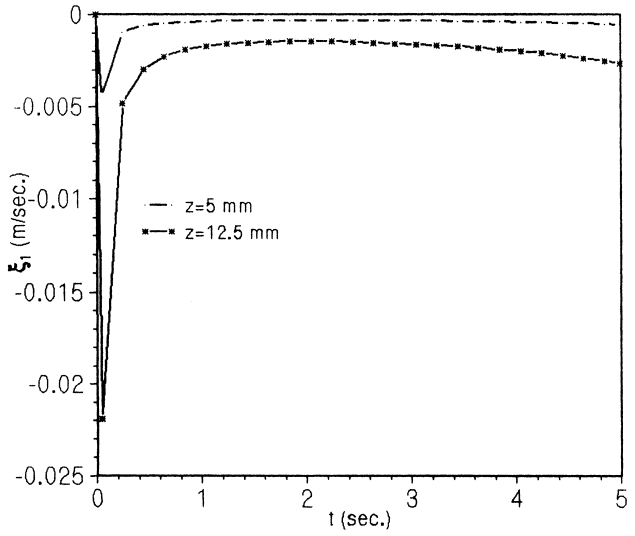

Fig. 15. Variation of the wall displacement with time for the parent aorta at $\beta = 30°$.

The results of the flow velocity in the daughter arteries for two different axial positions are presented in Fig. 6 at a particular instant of $t = 2$ s. One observes from the present results that the velocity profile remains parabolic near the apex corresponding to $z = 35$ mm and as one moves away from the flow divider, the profile gets perturbed largely towards the inner wall surface forming two separation zones, as indicated by the curve plotted for $z = 45$ mm. But the moment the body acceleration is withdrawn from the system under consideration, the profile also gets

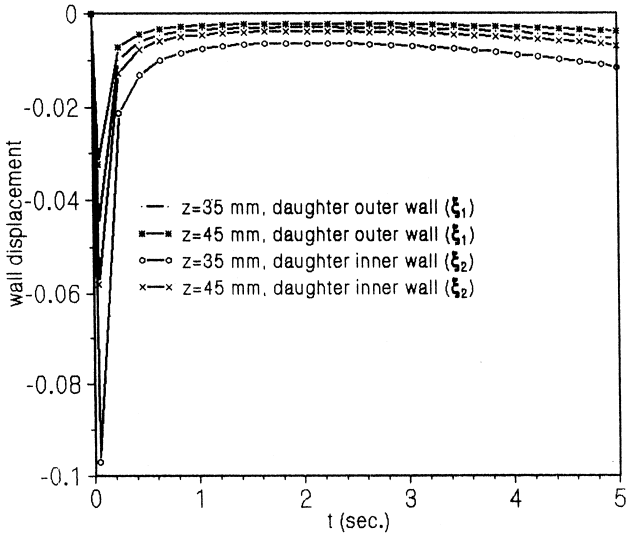

Fig. 16. Variation of the wall displacement with time for the daughter arteries at $\beta = 30°$.

distorted considerably towards the inner wall surface while a stationary zone is formed at the outer wall vicinity. The profile corresponding to a rigid artery however remains parabolic where no back flow takes place near the inner wall and no stationary zone is formed towards the outer wall. Such important characteristics are also absent in the steady flow consideration. Thus one may conclude from the present results that the flow unsteadiness has strong influences on flow separation zones while the steady flow assumption does not give an accurate picture of the actual flow behaviour in the aortic bifurcation.

Fig. 7 exhibits the results of the wall shear stress distributed over the parent aorta in the presence of stenosis for different time periods together with the influence of the body acceleration and the severity of the stenosis on them. One may note that for all times the wall shear stress becomes maximum at the critical site where the parent aorta assumes its maximum constriction and in the vicinity of which a separation zone is detected. Moreover, for all the times considered in the present results the stresses are relatively higher proximal to maximal stenosis and lower distal to the stenosis due to flow separation. When the body acceleration is not taken into account in the flow mechanism the stress gets enhanced significantly throughout the arterial segment with a large flow separation zone occupying most part of the constricted area. The symmetrical portion of the stress curve corresponding to the presence of stenosis becomes a straight line with constant stress in the absence of the constriction. If the severity of the stenosis present in the parent arterial lumen is raised from 40% to 60% the stress gets enhanced significantly causing the formation of a still larger flow separation zone in the constricted region as observed from the top most curve of the present figure. Thus both the external body acceleration and the severity of the stenosis affect the wall shear stress significantly throughout the stenotic region of the parent aorta. The present results indicate the waxing and waning of separation zones near the stenosis throughout the pulsatile flow has been delineated as a function of stenosis severity and such findings agree well with that of Clark and Robertson [10] who computed the effects of the severity of the stenosis for unbalanced simple-pulsatile bifurcation flow.

The distribution of the shear stress over the outer and the inner wall of the daughter artery for different time periods together with the effects of body acceleration, the distensibility of the vessel wall and the flow steadiness on them are displayed in Figs. 8 and 9. One may record here that there are two distorted shear stress regions – one on the outer wall peaking at a point immediately distal to the lateral junction and the other on the inner wall peaking at a point distal to the flow divider or the apex. This observation is in good agreement again with that of Lou and Yang [8]. There have been two major hypotheses that relate to a possible hemodynamic role in atherogenesis – one is the low shear stress pointed out by Caro et al. [19] and the other is the high shear stress reported by Fry [20]. One may also notice from the present figures that the outer wall shear stress increases gradually from the vertex and it forms several recirculation zones in the vicinity of $z = 50$ mm followed by the sharply increasing positive value while it maintains negative stress on the inner wall experiencing a disturbance near $z = 50$ mm. If one disregards the external body acceleration, the shear stress appears to experience relatively smaller disturbances on both the outer and the inner walls of the daughter arteries. When the distensibility of the vessel wall is completely ignored, the stresses on both the inner and outer walls are reduced considerably to the unperturbed values as shown in the present figures. The corresponding steady state values indicate uniform distributions on both the outer and inner walls with a little deviation on the outer wall and almost no deviation on the inner wall from those for a rigid artery. Here too, both the vessel wall distensibility and the body acceleration in the present flow mechanism play important role to the generation of high and low shear stress regions. It is worth while to mention that the sign of the wall shear stress becomes positive when the flow is forward and negative when the stream is reversed.

Fig. 10 shows the variation of the flow rate with time spanned over six cardiac cycles at a particular location of $z = 12.5$ mm where the constriction of the parent aorta is maximum in the presence of external body acceleration. The flow rate appears to get accelerated rapidly in the systolic phase and decelerated in the diastolic phase of the first cardiac cycle and then it gradually follows a slightly upward trend with little fluctuations for the rest of the time. In the absence of the stenosis, the flow rate gets enhanced significantly for the entire time range considered here and the peak flow rate in the systolic phase of the first cardiac cycle gets doubled to that for the constricted aorta where the flow velocity is essentially lowered. The deviation of the results thus obtained clearly estimates the effects of stenosis on the flow rate in the parent aorta bifurcating into the daughter arteries under consideration. Besides this, there is also an increasing trend of the flow rate much to the systolic phase of the first cycle and meagre to the rest of the time in the absence of wall motion. Thus the vessel wall distensibility helps reducing the peak flow rate to a considerable extent. The corresponding steady state values also reveal higher flow rate at the onset of the systolic phase till time $t = 0.4$ s and thereafter follow the usual trend of unperturbed path for all the times. Moreover, the flow rates in the daughter artery are also influenced by vessel wall distensibility, the body acceleration and the unsteadiness of the bifurcated flow as recorded in Fig. 11. The flow rate in the daughter arteries is found to be higher than that in the parent aorta in general and it is accelerated more in the absence of whole body acceleration than that in the presence of body acceleration, in particular. One may note here that the flow rate becomes entirely positive due to forward flow while its direction gets reversed in the steady state at $z = 45$ mm, a location away from the apex. The results of Figs. 10 and 11 possess a common feature that the flow rate curves become steady to some extent immediately after expiry of the first cardiac cycle.

The bifurcation angle claims to have a significant role in the characteristics of the flow rate for the daughter artery at the same critical location as is evident from Fig. 11(a) and (b). One observes that for $\beta = 68^\circ$, the results representing flow rate are entirely positive due to forward flow, they become entirely negative for $\beta = 70^\circ$ due to flow reversal and the separation zone is detected in the results for a critical value of $\beta = 69^\circ$.

Fig. 12 records the behaviour of the time-variant wall shear stress in the parent aorta at $z =$ 12.5 mm corresponding to its maximum narrowing. Three more curves are also plotted in this figure: (i) in the absence of any constriction; (ii) in the absence of the wall motion and (iii) in the steady state condition as noted with distinguishable marks. All these curves have their respective peaks at the onset of the cardiac cycle followed by a sharp fall to become minimum at the end of the first cardiac cycle and then they remain almost invariant for the rest of the time excepting a marginal increasing trend towards the large passage of time. It may be noted that the stress curve reverses its direction in the absence of arterial constriction and the stress disturbances disappear after the expiry of the first cardiac cycle. It has been suggested that the the change of shear stress direction or amplitude within a cardiac cycle may have some relevance to atherogenesis (cf. McDonald [21]). It has also been speculated by Fischer et al. [22] that the increased collagen production resulting from the pulsatile wall stretch due to pulsatile pressure gradient may be an initiating event in vessel wall injury leading to atherogenesis. Thus the findings of the present figure agree well with this hypothesis and perhaps it would help understanding the development of arterial diseases.

The variations of the wall shear stress with time for both the daughter outer and inner walls are depicted in Figs. 13 and 14 at $\beta = 30^0$. These figures also include the corresponding results for a rigid artery, without body acceleration and for steady flow condition. The stress characterizes to be positive on the outer wall and negative on the inner wall with much higher amplitudes inducing flow separation on both the inner and the outer wall of the branch arteries. The peak stress on the inner wall is found to be considerably higher than that on the outer wall irrespective of taking the body acceleration into account. On the other hand the wall distensibility induces flow reversal during the early period of a flow cycle, however, it restricts them during the second half of the cycle. The distensible bifurcation experiences shear stresses lower to a considerable extent than those of a rigid bifurcation at both the inner and outer wall of the brunch artery. This observation does agree qualitatively well with [8]. The corresponding steady flow analysis indicates the enhancement of the stresses both on the parent aorta (cf. Fig. 12) and the outer wall of the branch artery while on the inner wall of the daughter artery the stresses are reduced considerably.

Finally, the concluding Figs. 15 and 16 present the time variations of the wall displacements for the parent aorta and the daughter arteries with $\beta = 30^\circ$. Two specific locations of $z = 5$ and 12.5 mm have been chosen at the respective sites for the onset of the stenosis and for the maximum constriction in the parent aorta in order to examine the behaviour of wall displacement with time. Another two different sites of $z = 35$ and 45 mm have been selected – one at the flow divider and the other away from it in the daughter arteries. During the early period of the flow cycle the wall expansion becomes maximum which tends to induce flow reversals while vessel wall contraction tends to restrict them during the diastole. The amount of displacement becomes higher at the maximum narrowing of the parent aorta than at the onset of the stenosis so long as their magnitudes are concerned. In the daughter arteries the inner wall displacements are found to be higher than those of the outer wall at both the specific locations. Such characteristics of the vessel wall

distensibility resembles those of the flow rates and the shear stresses, which may play important role in the mechanism for atherosclerosis.

Acknowledgements

The authors are grateful to the Council of Scientific and Industrial Research for providing the financial assistance to carry out the present work.

Appendix A

The coefficients f_i $(i = 1, 2, 3, 4,)$ involved in Eq. (20) have got their expressions given by

$$f_1 = \left[\frac{K_1^{\theta}(0)}{\bar{R}^2} + \frac{1}{\bar{R}}(M_0 s^2 + C_r s + K_r)\right]\left[1 + \left(\frac{\mathrm{d}\bar{R}}{\mathrm{d}z}\right)^2\right]^{-1/2},$$

$$f_2 = \frac{\bar{p}_1}{\bar{R}}\left[1 + \left(\frac{\mathrm{d}\bar{R}}{\mathrm{d}z}\right)\right]^{-1/2} - \bar{p}_1\frac{\mathrm{d}^2\bar{R}}{\mathrm{d}z^2}\left[1 + \left(\frac{\mathrm{d}\bar{R}}{\mathrm{d}z}\right)^2\right]^{-3/2},$$

$$f_3 = \frac{1}{\bar{R}}\left[1 + \left(\frac{\mathrm{d}\bar{R}}{\mathrm{d}z}\right)^2\right]^{-1/2}(M_0 s^2 + C_l s + K_l)\frac{\mathrm{d}\bar{R}}{\mathrm{d}z},$$

$$f_4 = \frac{\mathrm{d}^2\bar{R}}{\mathrm{d}z^2}\left[1 + \left(\frac{\mathrm{d}\bar{R}}{\mathrm{d}z}\right)^2\right]^{-3/2}K_1^z(0).$$

The expressions for the coefficients g_{1k} $(k = 1, 2, 3, 4)$ appearing in Eq. (21) should be read as

$$g_{11} = \bar{R}K_1^z(0),$$

$$g_{12} = \left[K_1^z(0) - \left\{\frac{K_1^{\theta}(0)}{\bar{R}} + (M_0 s^2 + C_l s + K_l)\right\}\frac{f_4}{f_1}\right]\frac{\mathrm{d}\bar{R}}{\mathrm{d}z},$$

$$g_{13} = \left[-\frac{K_1^{\theta}(0)}{\bar{R}} - (M_0 s^2 + C_r s + K_r)\right]\frac{f_3}{f_1}\frac{\mathrm{d}\bar{R}}{\mathrm{d}z} - (M_0 s^2 + C_l s + K_l),$$

$$g_{14} = \left[-\frac{K_1^{\theta}(0)}{\bar{R}} - (M_0 s^2 + C_r s + K_r)\right]\frac{f_2}{f_1}\frac{\mathrm{d}\bar{R}}{\mathrm{d}z}.$$

The expression for the coefficients $a_{i,j}$, $b_{i,j}$ and $c_{j,j}$ in Eq. (35) should be used as

$$a_{i,j} = \mu\left\{\frac{1}{(\bar{R}_i\Delta x)^2} - \frac{1}{\bar{R}_i(x_j\bar{R}_i + \bar{R}_{2i})2\Delta x}\right\} - \frac{\rho}{2\Delta x\bar{R}_i}\left\{-R_{20i} + s\bar{R}_{2i} + x_j(-R_{0i} + s\bar{R}_i)\right\},$$

$$b_{i,j} = -\frac{2\mu}{\bar{R}_i^2(\Delta x)^2} - \rho s$$

and

$$c_{i,j} = \mu\left\{\frac{1}{(\bar{R}_i\Delta x)^2} + \frac{1}{\bar{R}_i(x_j\bar{R}_i + \bar{R}_{2i})2\Delta x}\right\} + \frac{\rho}{2\Delta x\bar{R}_i}\{-R_{20i} + s\bar{R}_{2i} + x_j(-R_{0i} + s\bar{R}_i)\}.$$

References

[1] S. Chakravarty, P.K. Mandal, An analysis of pulsatile flow in a model aortic bifurcation, Int. J. Eng. Sci. 35 (1997) 409–422.

[2] D.W. Liepsch, S.T. Moravec, Pulsatile flow of non-Newtonian fluid in distensible models of human arteries, Biorheology 21 (1984) 571–586.

[3] D.W. Liepsch, in: D.W. Liepsch, S. Karger, Basel (Eds.), Effect of Blood Flow Parameters on Flow Patterns at Arterial Bifurcations: Studies in Models, in Blood Flow in Larger Arteries: Applications to Atherogenesis and Clinical Medicine, vol. 63, 1990.

[4] Z. Lou, W.J. Yang, Biofluid dynamics at arterial bifurcations, Crit. Rev. Biomed. Engng. 19 (1992) 455–493.

[5] D.N. Ku, D.W. Liepsch, The effects of non-Newtonian viscoelasticity and wall elasticity on flow at a 90° bifurcation, Biorheology 23 (1986) 359–370.

[6] D.D. Duncan, C.B. Bargeron, S.E. Borchardt, O.J. Deters, S.A. Gearhart, F.F. Mark, M.H. Friedman, The effect of compliance on wall shear in casts of a human aortic bifurcation, J. Biomech. Eng. Trans. ASME 112 (1990) 183–188.

[7] P.J. Reuderink, H.W. Hoogstraten, P. Sipkema, B. Hillen, N. Westerhof, Linear and non-linear one-dimensional models on pulse wave transmission at high womersley numbers, J. Biomech. 22 (1989) 819.

[8] Z. Lou, W.J.A. Yang, Computer simulation of the blood flow at the aortic bifurcation with flexible walls, J. Biomech. Eng. Trans. ASME 115 (1993) 306–315.

[9] D.J., Patel, R.N. Vaishnav, Basic Haemodynamics and its Role in Disease Processes, University Park Press, Baltimore, 1980.

[10] M.E. Clark, J.M. Robertson, L.C. Cheng, Stenosis severity effects for unbalanced simple-pulsatile bifurcation flow, J. Biomech. 16 (1983) 895–906.

[11] D.J. Patel, D.L. Fry, Longitudinal tethering of arteries in dogs, Circ. Res. 19 (1966) 1011–1021.

[12] H.B. Atabek, Wave propagation through a viscous tethered, initially stressed, orthotropic elastic tube, Biophys. J. 8 (1968) 626–646.

[13] A.C. Burton, Physiology and Biophysics of the Circulation: Introductory Text, Year Book Medical Publisher, Chicago, 1966.

[14] W.R. Milnor, Haemodynamics, Williams and Williams, Baltimore, 1982.

[15] I. Mirsky, Wave propagation in a viscous fluid contained in an orthotropic elastic tube, Biophys. J. 7 (1967) 165–186.

[16] J.T. Young, R.N. Vaishnav, D.J. Patel, Non-linear anisotropic viscoelastic properties of canine arterial segments, J. Biomech. 10 (1977) 549–559.

[17] T. Fukushima, T. Homma, K. Harakawa, N. Sakata, T. Azuma, Vortex generation in pulsatile flow through arterial bifurcation models including the human carotid artery, J. Biomech. Eng. 110 (1988) 166–171.
[18] Z. Lou, W.J. Yang, A computer simulation of the blood flow at the aortic bifurcation, Bio-Med. Mater Eng. 1 (1991) 173–193.
[19] C.G. Caro, J.M. Fitz-Gerald, R.C. Schroter, Atheroma and arterial wall shear: Observation, correlation and proposal of a shear dependent mass transfer mechanism for atherogenesis, Proc. R. Soc. Lond. B177 (1971) 109–159.
[20] D.L. Fry, Acute vascular endothelial changes associated with increased blood velocity gradients, Circ. Res. 22 (1968) 165–197.
[21] D.A. McDonald, Blood Flow in Arteries, 2nd ed., Edward Arnold, London, 1974.
[22] G.M. Fischer, M.L. Swain, K. Cherian, Pulsatile distension and vascular collagen synthesis in the rabbit, Blood Vessels 17 (1980) 215.